Photonic Integrated Device for Chaos Applications in Communications

A. Argyris,[1,2] M. Hamacher,[3] K. E. Chlouverakis,[1] A. Bogris,[1] and D. Syvridis[1]

[1]*Optical Communications Laboratory, Department of Informatics and Telecommunications, University of Athens, Panepistimiopolis, Illisia, 15784 Athens, Greece*

[2]*Department of Computer Engineering, Telecommunications and Networks, University of Thessaly, 38221 Volos, Greece*

[3]*Fraunhofer Institute for Telecommunications, Heinrich-Hertz-Institute, 10587 Berlin, Germany*

(Received 20 March 2008; published 16 May 2008)

A novel photonic monolithic integrated device consisting of a distributed feedback laser, a passive resonator, and active elements that control the optical feedback properties has been designed, fabricated, and evaluated as a compact potential chaotic emitter in optical communications. Under diverse operating parameters, the device behaves in different modes providing stable solutions, periodic states, and broadband chaotic dynamics. Chaos data analysis is performed in order to quantify the complexity and chaoticity of the experimental reconstructed attractors by applying nonlinear noise filtering.

DOI: 10.1103/PhysRevLett.100.194101 PACS numbers: 05.45.Vx, 05.45.Tp, 42.65.Sf, 42.82.Bq

The exigency for increased security in data exchange using the fledging technology of optical communication networks, which is used nowadays as the dominant backbone data transmission infrastructure, has directed a considerable part of research to physical layer data encryption techniques [1–3]. Synchronization in nonlinear and chaotic systems [4–7] has established a revolutionary approach in securing data communications over fiber transmission, by encoding the messages over chaotic optical carriers. Based on optical feedback [8,9], optical injection [10], and optoelectronic feedback [11] techniques applied to semiconductor lasers, various configurations of transmitters have been proposed and implemented, providing high-dimensional chaotic carriers capable of message encryption [1]. The latter takes advantage of the off-the-shelf fiber-optic technology resulting in rather cumbersome devices, impractical for commercial use.

The miniaturization of the above configurations through photonic integration appears very attractive, albeit scarce, considering the efficiency of specifically designed photonic integrated circuits (PICs) to generate nonlinear dynamics [12–15]. In [12] monolithic colliding-pulse mode-locked lasers exhibited nonlinear behavior, from cw operation to self-pulsations and mode-locking, for the full range of the control parameters. In [13] a semiconductor laser, followed by a phase section and an active feedback element, forms a very short complex photonic circuit that provides several types of dynamics and bifurcations under optical feedback strength and phase control. However, only multiple-mode beating operation may transit the dynamics beyond a torus breakup with possible chaotic components. A simplified version of the aforementioned PIC, omitting through the active feedback element, was found to generate only distinct-frequency self-pulsations [14]. Very recently, using an integrated colliding-pulse mode-locked semiconductor laser, the existence of nonlinear dynamics and low-frequency chaos in PICs was demonstrated by controlling through only the laser injection current [15]. Albeit all the aforementioned integrated devices present interesting nonlinear and chaotic behavior, they are not suitable for generating high-dimensional broadband chaotic emission for message encryption applications. The ultimate objective of this work is to exploit the complex dynamics of such devices in a way that will fulfill the criteria for efficient data encryption on the physical layer.

In this Letter, we present a novel photonic integrated circuit, capable of generating high-dimensional broadband chaos. The proposed device incorporates the fundamental principles of the all-optical feedback theory, using elements that provide the capability to control the chaotic properties of the optical emission accurately and reproducibly. It consists of four successive sections (Fig. 1): a distributed feedback (DFB) InGaAsP semiconductor laser operating at 1561 nm, followed by a gain-absorption section (GAS), a phase section (PH) and a 1 cm long passive waveguide. The passive waveguide is grown by a selective area epitaxial growth. The overall resonator length is de-

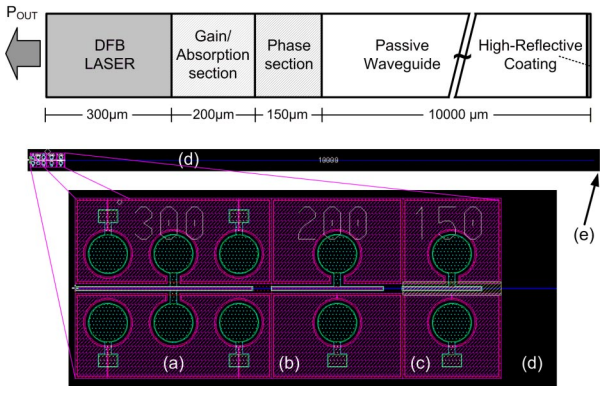

FIG. 1 (color online). (Top) Schematic diagram of the photonic integrated device. (Bottom) Detail of the mask design of the integrated device: (a) InGaAsP DFB laser; (b) gain-absorption section; (c) phase section; (d) passive waveguide. While the laser facet is anti-reflection coated, the end of the waveguide is highly reflective coated (e). The lengths of the different sections are in micrometers.

fined by the internal laser facet and the chip facet of the waveguide which is highly reflective coated (HRC) ($R = 95\%$) and includes the GAS and PH. A criterion of the selection of the cavity length is the ability of the device to produce chaotic attractors with high complexity. The selected length of 1 cm provides an increased effective feedback round-trip time, therefore enhancing the probability to encounter fully chaotic behavior, as also predicted numerically in [16,17] using a modified Lang-Kobayashi set of rate equations. The integration of a GAS emerges from the requirement to control the optical feedback strength. Taking into account that the PIC's optical feedback is determined by its total internal losses and the passive waveguide facet reflectivity, the GAS provides a twofold operation:

In cases where the desirable feedback values surpass the provided feedback of the passive cavity (GAS and PH unbiased), positive biasing of the GAS—acting thus as a semiconductor optical amplifier (SOA)—provides the ability to amplify the optical field emitted from the inner facet of the laser and thus increase the feedback strength. In cases where lower values of optical feedback are needed, the GAS can be reverse biased and acts as a variable optical attenuator (VOA). Consequently, a very wide range of optical feedback values can be set and thus various types of dynamics can be generated. The integration of a PH emerges from the requirement to adjust the phase of the optical feedback field [18]. While the GAS affects both intensity and the phase of the feedback signal, the PH allows for fine-tuning that can almost continuously go over beyond 2π, even several multiples of it. This is crucial for controlling the dynamics performance of lasers with external short-cavity optical feedback, since the response of the laser is triggered by a coherent delayed optical field.

The total internal losses of the fabricated device and the reflectivity of the external cavity coating determine practically the amount of the optical feedback that is driven into the laser section. The internal losses are attributed to the different section interfaces and the waveguide losses. Considering a zero-biased GAS, the above internal losses are measured 9 dB per pass approximately, corresponding to an optical feedback power ratio of 1.6%. The losses have been estimated by measuring the light coming out from the HRC end of the waveguide. For a measured value of optical output of the laser and a given reflectivity of the HRC facet the total losses can be easily estimated. Short external cavities (lengths up to a few centimeters) require a relatively strong optical feedback in order to generate high-dimensional dynamics. In our case, the integrated GAS will provide the prerequisite gain to strengthen the optical signal or compensate for the additional losses inside the cavity providing the desirable value of the optical feedback.

According to our numerical calculations (using the rate-equation model in [16]) and experimental measurements, the laser biasing current is not crucial for achieving enhanced nonlinear dynamics when it is kept well above threshold. When the DFB laser is biased at $3I_{TH}$ ($I_{TH} = 10.6$ mA) different types of dynamics can be observed depending on GAS and PH operation. Four different operating regions have been identified for specific values of GAS biasing:

(a) GAS reverse biasing = VOA operation.—When the GAS is reverse biased, e.g., at -0.4 V, the total attenuation that the emitted power experiences after a round trip within the cavity is enhanced to 23 dB. Here, the optical power feedback ratio was estimated to be 0.5%. Only limit cycle dynamics or stable solutions (cw operation) are observed excluding any chaos dynamics.

(b) $I_{GAS} = 0$ mA.—The dynamics of the output signal differs considerably when altering the cavity phase through the PH current I_{PH}. Such a behavior has been previously reported [16] for the short-cavity regime, as a manifestation of a strong dependence of the largest Lyapunov exponent on the feedback phase value. This phase dependence was also experimentally observed in [17], where the short cavity was formed by an aspheric lens collimating the laser beam and a semitransparent dielectric mirror. By increasing I_{PH} the observed dynamic states are periodically repeated every 6.2 mA, indicating a cycle of 2π phase change. The different dynamic states, which include limit cycles and chaotic states, are depicted in Fig. 2 and emerge for different phase values. In some narrow phase current regions two intense peaks are observed at 3.3 and 6.6 GHz, while the rest spectral components lay almost just above the noise floor [Figs. 2(a) and 2(e)]. These peaks correspond to the external cavity modes; however, their frequencies shift slightly with phase tuning. A similar observation was reported in [17], where the phase dependence of the dynamics was exhibited as well. The physical explanation for this frequency shift is the dependence of the frequency of the external cavity modes on the feedback phase according to stability analysis theory [19]. In other phase current regions, various limit cycle conditions arise: the first peak may be suppressed entirely or additional peaks of moderate power may arise [Fig. 2(b)]. There is also a range for the phase section current values (from 5.4 to 5.9 mA) in which the device operates in the coherence collapse regime providing a chaotic output, as revealed from the phase plots of Figs. 2(c) and 2(d). In this operating region the radio-frequency spectrum of the output signal becomes broadband and extends up to the cutoff frequency of the optical receiver (around 8 GHz). The frequency peaks are now much less intense, however still distinguishable from the rest strengthened spectral components.

(c) $I_{GAS} = 5$ mA = SOA operation.—When the GAS is slightly positively biased (e.g., 5 mA), the provided gain in the cavity compensates the internal losses, increasing the optical power feedback ratio to 2.8%. In this case, there is only a single phase condition in which an intense peak at 6.3 GHz emerges in the microwave spectrum. The rest phase region was found to provide only broad-spectrum

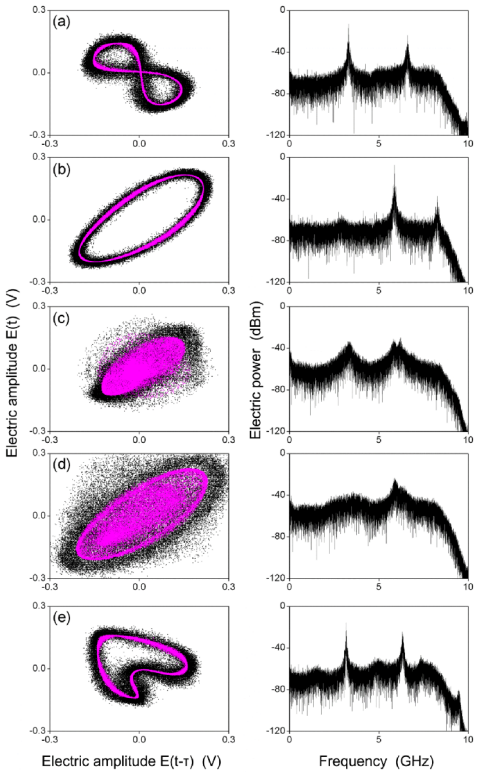

FIG. 2 (color online). Feedback phase dependence: Experimental phase plots (left column) and corresponding microwave spectra (right column) of the device output for $I = 3I_{\mathrm{TH}}$ and $I_{\mathrm{GAS}} = 0$ mA. From (a) to (e), $I_{\mathrm{PH}} = 3.3$, 4.8, 5.5, 5.9, and 6.9 mA. The colored (gray scale) trace denotes the filtered attractor.

chaotic dynamics, therefore deteriorating the phase dependence.

(d) $I_{\mathrm{GAS}} = 10$ mA $=$ SOA *operation.*—When the GAS is moderately biased (e.g., 10 mA), providing now 1.3 dB additional gain compared to the previous condition (c), the optical power feedback ratio rises to 3.3% and the output signal now is fully chaotic and independent of any phase condition (Fig. 3). Any further increase in the GAS current does not provide any alteration in the characteristics of the chaotic spectrum.

In order to investigate the dynamics of the experimentally resolved time series, chaos data analysis is performed

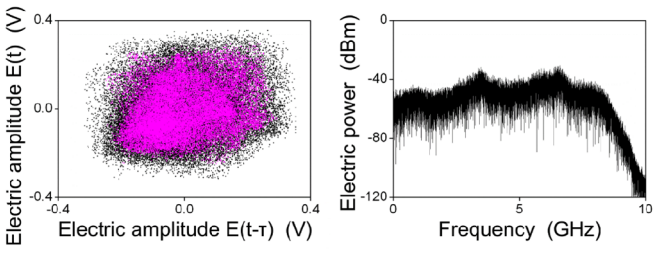

FIG. 3 (color online). Experimental phase plots (left panel) and corresponding microwave spectra (right panel) of the device output for $I = 3I_{\mathrm{TH}}$, $I_{\mathrm{GAS}} = 10$ mA and $I_{\mathrm{PH}} = 2.9$ mA. The colored (gray scale) trace denotes the filtered attractor.

since the prevalent idea is to identify the complexity of the strange attractors and substantiate their suitability for encryption applications. Experimental data, and especially laser series, are always noise contaminated and may lead to false claims regarding chaos identification or even to aver erroneous estimates of the correlation dimension and Kolmogorov entropy calculation [20,21]. In order to visualize the substantial dynamics for every recorded time - series, it is prudent to enroll noise-reduction methods. For complex chaotic data, state-space averaging is considered as one of the most apt and intricate methods (in contrast to linear filtering) in order to remove nondeterministic components from a series, to ameliorate visually the geometrical structure of the reconstructed attractor (Figs. 2 and 3), and to illuminate the underlying mechanisms. Following this method, one has to postdict or hindcast with *a posteriori* knowledge of all N points, by averaging the segments of the data in which a window of $\pm m$ points on each side of X_n (the matrix containing each experimental data) is close to it in state space [22,23]:

$$\tilde{X}_n = \frac{\sum_{k=m}^{N-m} X_n W_n(k)}{\sum_{k=m}^{N-m} W_n(k)}, \quad \text{where}$$
$$W_n(k) = \exp\left[\frac{-\sum_{i=-m}^{m}(X_{k-i} - X_{n-i})^2}{\sigma_N^2}\right]. \tag{1}$$

The filtered series is denoted by $\tilde{X}_n$, and the value of m used herein was $m = 9$. The parameter σ_N (the standard deviation of noise), which is evidently unknown, is optimized by adjusting it to the best in-sample fit [23]. The noise-filtered attractors are superimposed to the initially recorded ones shown in color (or gray scale) in Figs. 2 and 3. The delay τ is defined as the time value for which the autocorrelation function decays to the inverse Euler constant e^{-1} [24]. The applied noise-reduction method herein follows the rationale that the geometrical topology and dynamics maintain their unmitigated complexity and the variance of noise is smaller than the signal.

The correlation dimension D_2 and Kolmogorov entropy K_2 were calculated with the Grassberger-Procaccia method [25]. For a detailed description of this method, see [21,23,25–27]. For the zero-biased GAS (subsection *b*) chaos data analysis is performed in Fig. 4. The depicted values of D_2 (black solid line) and K_2 (black dash-dotted line) correspond to the noise-filtered attractors. The calculation of complexity is patently arduous and misleading for the original attractors, especially when periodic states are concerned. Because of the noise presence resulting in the augment of loss of correlation between neighbor points, the periodic states are incorrectly evaluated as chaotic ($D_2 > 2$ and $K_2 > 0$). Therefore, the latter are omitted and D_2 is plotted (Fig. 4, red or gray line) only for the chaotic states. All cases that correspond to limit cycle dynamics in Fig. 4 are characterized by a low correlation dimension D_2—approximately close to unity taking into account the stochastic noise sources—and zero entropy K_2. However, for the chaotic operation achieved for $5.4 < I_{\mathrm{PH}} < 5.9$ the

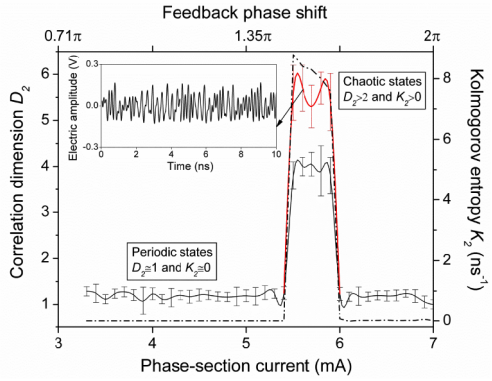

FIG. 4 (color online). Correlation dimension D_2 and Kolmogorov entropy K_2 as the feedback phase varies for $I = 3I_{\mathrm{TH}}$ and $I_{\mathrm{GAS}} = 0$ mA. Red (gray) denotes the value of D_2 for the chaotic nonfiltered original series, the black solid line denotes D_2 for the filtered series, and the black dash-dotted line denotes K_2 for the filtered series. The inset depicts an experimental chaotic time series for $I_{\mathrm{PH}} = 5.5$ mA.

correlation dimension and the Kolmogorov entropy now are considerably increased up to $D_2 \approx 6$ and $K_2 = 8.8\ \mathrm{ns}^{-1}$, respectively.

For the case of the filtered time series in Fig. 3 [subsection (d)], the dimension was calculated $D_2 = 4.8 \pm 0.3$ together with $K_2 \approx 10\ \mathrm{ns}^{-1}$, values higher than those calculated in Fig. 4 for the zero-biased GAS. This result is expected due to the increased feedback strength. For the originally captured experimental time series, dimension could not be estimated since the correlation integral was increasing with the embedding dimension (and therefore assumed $D_2 > 6$) whereas K_2 remained unaltered. These results verify the work in [26] for entropy invariability and dimension alteration with applying noise reduction in chaotic cases. The filter is not able to destroy or create information by itself but is able to provide the correct geometrical morphology of the attractor by mitigating the spuriously increased dimension aright. For periodic cases and stable solutions, but also for chaotic cases that are amply contaminated with noise of comparable amplitude [27], K_2 is affected since noise mimics a chaotic attractor that actually is a noisy one (K_2 and $D_2 \rightarrow \infty$) but with limited bandwidth (therefore K_2 and D_2 have finite spurious values).

The trend nowadays in the next-generation optical communication systems is towards robust and sophisticated integrated photonic circuits. With respect to that, a novel photonic integrated circuit that is capable of producing broadband high-dimensional chaotic dynamics was designed, fabricated, and investigated in terms of complexity and chaoticity. Dynamics can be easily controlled experimentally via the phase current and feedback strength, therefore establishing this device as a compact integrated chaos emitter. Since the dynamics are well identified, the advantages of the proposed photonic integrated device may be fully exploited to our benefit with a fervent expectation for applications to secure chaos-encoded optical communications.

This work has been supported under EC Project No. PICASSO IST-2006-34551.

[1] A. Argyris *et al.*, Nature (London) **437**, 343 (2005).
[2] R. Roy, Nature (London) **438**, 298 (2005).
[3] T. Schmitt-Manderbach *et al.*, Phys. Rev. Lett. **98**, 010504 (2007).
[4] L. M. Pecora and T. L. Carroll, Phys. Rev. Lett. **64**, 821 (1990).
[5] K. M. Cuomo, A. V. Oppenheim, and S. H. Strogatz, IEEE Trans. Circuits Syst. II **40**, 626 (1993).
[6] P. Colet and R. Roy, Opt. Lett. **19**, 2056 (1994).
[7] C. R. Mirasso, P. Colet, and P. Garcia-Fernandez, IEEE Photonics Technol. Lett. **8**, 299 (1996).
[8] V. Annovazzi-Lodi, S. Merlo, M. Norgia, and A. Scire, IEEE J. Quantum Electron. **38**, 1171 (2002).
[9] S. Sivaprakasam, P. S. Spencer, P. Rees, and K. A. Shore, IEEE J. Quantum Electron. **38**, 1155 (2002).
[10] H.-F. Chen and J.-M. Liu, Phys. Rev. E **71**, 046216 (2005).
[11] M. Peil, L. Larger, and I. Fischer, Phys. Rev. E **76**, 045201 (2007).
[12] T. Franck, S. D. Brorson, A. Moller-Larsen, J. M. Nielsen, and J. Mork, IEEE Photonics Technol. Lett. **8**, 40 (1996).
[13] S. Bauer, O. Brox, J. Kreissl, B. Sartorius, M. Radziunas, J. Sieber, H.-J. Wünsche, and F. Henneberger, Phys. Rev. E **69**, 016206 (2004).
[14] O. Ushakov, S. Bauer, O. Brox, H.-J. Wünsche, and F. Henneberger, Phys. Rev. Lett. **92**, 043902 (2004).
[15] M. Yousefi, Y. Barbarin, S. Beri, E. A. J. M. Bente, M. K. Smit, R. Nötzel, and D. Lenstra, Phys. Rev. Lett. **98**, 044101 (2007).
[16] R. Vicente, J. Dauden, P. Colet, and R. Toral, IEEE J. Quantum Electron. **41**, 541 (2005).
[17] T. Heil, I. Fischer, W. Elsässer, B. Krauskopf, K. Green, and A. Gavrielides, Phys. Rev. E **67**, 066214 (2003).
[18] Y. Ikuma and J. Ohtsubo, IEEE J. Quantum Electron. **34**, 1240 (1998).
[19] J. Mork, B. Tromborg, and J. Mark, IEEE J. Quantum Electron. **28**, 93 (1992).
[20] E. Ott, *Chaos in Dynamical Systems* (Cambridge University Press, Cambridge, England, 1993).
[21] I. Fischer, O. Hess, W. Elsäβer, and E. Göbel, Phys. Rev. Lett. **73**, 2188 (1994).
[22] T. Schreiber, Phys. Rev. E **48**, R13 (1993).
[23] C. Sprott, *Chaos and Time Series Analysis* (Oxford University Press, Oxford, UK, 2003).
[24] J.-P. Eckmann and D. Ruelle, Rev. Mod. Phys. **57**, 617 (1985).
[25] P. Grassberger and I. Procaccia, Phys. Rev. Lett. **50**, 346 (1983).
[26] F. Mitschke, M. Moller, and W. Lange, Phys. Rev. A **37**, 4518 (1988).
[27] K. E. Chlouverakis, A. Argyris, A. Bogris, and D. Syvridis, Physica (Amsterdam) **237D**, 568 (2008).